Prediction of contact condition and surface damage by simulating variable friction coefficient and wear

A. Mäntylä[a,1,*], J. Hintikka[a], T. Frondelius[a,c], J. Vaara[a], A. Lehtovaara[b], J. Juoksukangas[b]

[a] *Wärtsilä Finland Oy, Järvikatu 2-4, P.O. Box 244, 65101 Vaasa, Finland*
[b] *Tampere University, Tribology and Machine Elements, Faculty of Engineering and Natural Sciences, P.O. Box 589, 33014 Tampere, Finland*
[c] *University of Oulu, Materials Engineering Laboratory, Finland*

Abstract

A simulation method to predict the reliability of clamped metal contacts under cyclic loading is presented. The main idea is to predict the development of contact condition of a joint by simulating a spatially variable coefficient of friction (COF) and wear. Frictional energy dissipation drives the COF evolution rule, and classic Archard's equation is employed as the evolution rule for wear depth. As both the COF and wear evolution are considered, the presented approach is capable of predicting changes in the contact condition over time. The approach is based on the Finite Element Method (FEM) and is generally applicable to industrial cases. The method is implemented as a subroutine to a FEM solver Abaqus to define a contact formulation in both normal and tangential directions. The subroutine allows full coupling between normal and tangential contact variables, which makes the approach robust also in complex industrial applications. As the effect of wear is described in the contact pressure calculation, there is no need for mesh modification. The presented approach was validated by simulating cylinder-on-plane configuration. The presented method provides similar results obtained with a simulation where geometry is updated due to wear. The results of the case study were qualitatively verified against a bolted joint type fretting experiment. The area of slip after stabilized COF distribution corresponds well with the experimental fretting scars. However, Archard's wear law seems to be limited, at least in partial slip cases, as it overestimates the amount of wear without considering entrapment of wear debris in the contact. A case study of medium speed combustion engine component is presented to show how the simulation method can be used in engine development to ensure reliable contact interfaces.

Keywords: Fretting, fatigue, contact, friction, wear, finite element method

1. Introduction

Fretting is small amplitude reciprocating surface sliding, and it may result in fretting fatigue and fretting wear. In fretting fatigue, cyclic surface stresses accelerate the crack initiation. Fretting wear is characterized by the occurrence of fine powdery wear debris, which tends to entrap inside the fretting contact. [1, 2, 3]

When designing critical engine components, in addition to accurate plain fatigue assessment [4, 5, 6], it is essential to prevent surface damage in the contact interfaces because fretting induced cracks can lead to unexpected and catastrophic failures. An example of connecting rod fretting failure in a large combustion engine can be found from reference [7]. In that case, there was some local slip in the shrink fit between the bearing bush and the housing, which caused fretting crack nucleation. While the propagation of the fretting-induced cracks can be evaluated using fracture mechanics [8, 9, 10, 11] and short crack theories [12], there is no generalized theory to quantify the surface damage that leads to fretting crack initiation. Ruiz fretting damage parameter (FDP) [13] and its enhancement [14] can be used to predict potential locations of the fretting damage, but their sensitivity to friction coefficient makes it

* *Email address:* antti.mantyla@wartsila.com (A. Mäntylä)
[1] Phone: +358503665329

challenging to define damage thresholds in general. This sensitivity can be seen, for example, in [15], where the Ruiz criterion and its enhancement is applied to a railway axle shrink fit with different COF and radial interference values.

It is also essential to prevent 'adhesion spots' or wear as they can harm the functionality of the joints and serviceability. Experiments show that fretting can induce cracks with a depth of millimeter even in nominally flat-on-flat steel contact with a relatively low contact pressure of 30 MPa without significant bulk stress or macroscale contact stress amplitude [16]. An example of fretting spots and cracking in a large engine component is shown in Fig.1. In this case, nominal fatigue loading at the cracked location was only 20% of the fatigue limit of the material, but still, the concentration of stresses in the formed adhesion spot led to fretting induced cracking. In these kinds of cases, the fatigue criteria based on plain fatigue tests and the assumption of ideal contact conditions are not very helpful in component level simulations. The damage prediction should include the effects of the contact parameters such as coefficient of friction (COF), slip, and possible wear. Jiménez-Peña et al. have used several multiaxial fatigue criteria and Fretting Fatigue Damage (FFD) parameter to predict the effect of pre-tightening force on fretting fatigue life of a bolted joint [17]. The FFD considers the slip and frictional shear stress and is the only criterion that is in agreement with the experimental results, showing that increased pre-tightening force leads to increased fretting fatigue life. In that case, the multiaxial criteria predict that increased pre-tightening force decreases the fretting fatigue life. It also has to be noted that in cases where the contact geometry itself causes high stress concentrations in the contact, as in cylinder or sphere against a plane case, fatigue based criteria can predict cracking as shown in [18, 19, 20, 21].

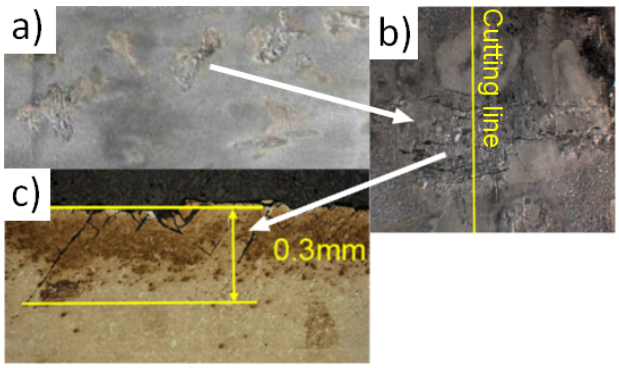

Figure 1: Fretting damage spots in a large contact interface (a), a fretting damage spot (b) and fretting induced cracks (c).

Friction and values of COF are important parameters affecting the severity of total fatigue load via contact stresses [3]. Also, the running condition (stick, partial-slip, and gross-sliding) is sensitive to the value of COF, contact geometry, and loads [22]. High COF, over unity, is usually measured in fretting. The high COF, combined with geometrical contact stress concentration, can explain fatigue cracking without cyclic bulk stress [23, 24]. Furthermore, it is well known that variable COF is present in the fretting conditions, and it is usually considered to be dependent on the number of load cycles. Sphere-on-plane and flat-on-flat gross slip experiments with quenched and tempered steel suggest that 'hardening' of friction occurs during the early stages of the experiment as COF increases rapidly and peaks at values between 1.3 (flat-on-flat) and 1.5 (sphere-on-plane). However, the initial 'hardening' is followed by 'softening' as COF gradually reduces and stabilizes to value of about 0.8 in both test configurations. [24, 25]. Stable frictional behavior can be achieved, although this requires that only a fraction of the available friction is utilized [26, 27]. Effects of variable friction [28] and non-uniform friction [29, 30] have been taken into account in the analysis of fretting experiments. For example, Yue et al. have obtained better results in a partial slip and early stages of a gross slip by defining COF as a function of cycles [28]. Naboulsi et al. modeled friction to be dependent on slip and normal pressure and obtained promising results [29]. Cheich et al. have proposed a so-called kinematic isotropic coefficient of friction (KI-COF), producing a sound match against the experimental results in a cylinder-on-plane configuration [30].

Loose and solid third body layers inside interface carry loads and contribute to the wear between the first bodies and friction via various velocity accommodation mechanisms [31]. The third body is especially crucial in fretting conditions because of typically low slip amplitude and closed contact [32]. Fretting wear experiments have revealed

that considerable size effects exist [33, 34], which can be explained by entrapment of wear debris and resulting velocity accommodation in them. Wear has an essential effect on the contact condition as it redistributes contact pressure and can reduce the clamping force, especially in the bolted joints or interference fits. Several authors have employed Archard's wear law to study the effects of wear in contacts [35, 36, 37]. Classic observation is that the fretting fatigue life is the lowest in the partial slip regime near the gross-sliding threshold. Experimental findings show that the fatigue life increases as a function of slip amplitude in the gross-sliding regime, which has been explained by wear erasing initiated cracks before propagation to the bulk material [38]. However, detailed modeling of Hertzian fretting conditions has revealed that fretting wear leads to increasing contact size, reducing surface pressure, and relocating the most severely stressed point [37]. Fretting wear has been studied in partial slip problems in [39, 40, 41]. For Hertzian line and point contacts, it has been shown that gradual wear of sliding region ultimately leads to a condition where the original stick zone carries all of the load [39, 40]. Plasticity in the model can lead to a gradually advancing wear area due to yielding at the edges of the stick zone [41].

Partial slip condition is prevalent in the contacts of real machinery and cannot always be avoided. From a machine design perspective, the effect of wear becomes essential as the loosening of the contact depends on the size of the worn area and stiffness of the clamping structure. Wear may reduce the load-carrying capacity and integrity of the joint, which consequently may lead to gross slip and total failure of the joint.

The development of modern medium-speed combustion engines is driven mainly by the fact that performance demands are increasing, and emission regulations become stricter all the time. In the engine development, this is seen as increasing loading level of the components and optimization of the structures. Especially with large engines, modern simulation methods are crucial as prototypes and full-scale testing are expensive. Wärtsilä has a long history in structural simulations starting with finite element method (FEM) at 1973 [42]. Today simulations are an integral part of the design process with the aim of "first-time-right" engine design and development [43]. Flexible multi-body simulation (MBS) methodology has been taken into use in Wärtsilä to be able to capture complicated dynamics of engine components [44, 45]. By using loadings from MBS, non-linear FEM analysis enables accurate simulation of stresses and contact behavior of component sub-assemblies [46].

In medium-speed combustion engine components, the contact interfaces are usually much larger compared to typical fretting experiments. In practice, uniform contact pressure and shear traction are rarely achieved in contacts of real components leading to spatially non-uniform conditions for the COF to evolve. The evolution of COF is history-dependent, and the average value has a strong effect on the gross slip limit of the contact. The evolution of COF in one place can affect slip or shear load in another place in the contact. Additionally, even if stable stick conditions are achieved, certain regions may already have been damaged. Even slight exposure for fretting may significantly impair the component's fatigue properties due to surface degradation and cracking [47]. Thus, there is a need for developing a model that considers non-uniform COF evolution and wear across the contact, and which can be used to utilize scientific laboratory findings in industrial-scale simulations. In this manuscript, a new COF evolution rule is presented where the value of COF increases as a function of frictional dissipation. The evolution of COF can be used as a fretting damage indicator based on the stable COF concept [26], where utilized COF (shear traction/contact pressure) has some safe and stable limit below which the fretting damage does not occur, and the contact stays in stable condition [26, 27]. Overall, this friction model has some analogy to material plasticity models, where the yield limit increases locally as a function of equivalent cumulative plastic strain. The approach is inspired by previous studies where experimental wear and friction findings have been implemented in the analysis of contact mechanical response [37, 28, 29, 30].

The novelty of this paper is that both the evolution of COF and wear are used to predict changes in the contact conditions, indicate the level of damage and assess the functionality of contacts under fretting conditions. The methodology is unique as it has been aimed for real component simulations. When the local COF value stays below the measured safe limit, it means that the location is stuck and safe. On the other hand, if the local COF reaches the limit value and sliding occurs, surface damage is expected.

2. Methods

2.1. Contact subroutine

To be able to simulate local friction evolution and wear, a subroutine (UINTER) was written to replace the standard contact formulation in commercial finite element solver Abaqus. Inside the routine, the solver suggests the

displacement increment in normal and tangential directions, and the user has to define the contact condition, traction vector, and its derivatives. The main advantage of this approach is that the user has full freedom to define contact physics, and no need to touch the higher-level numerical methods such as surface discretization or contact tracking. Wear is modelled by introducing a nodal gap value at each node in contact. This local gap value corresponds to the calculated wear depth and allows the penetration of contact nodes before any contact pressure is formed. Penalty formulation [48] was selected as a basis for the routine for two reasons: Firstly, real metal contacts have finite normal and tangential stiffness due to surface asperity interaction [49]. Secondly, the penalty method has better convergence in challenging contact problems than Lagrange multiplier method [48].

Normal pressure is defined as the product of overclosure (penetration) of the contacting surfaces and normal stiffness k_n. To consider the effect of wear on the normal pressure, the wear depth r is subtracted from the overclosure of unworn contact h. Practically this means that the contact surfaces can penetrate each other by the amount of wear before any normal pressure forms. The normal pressure p is thus given by

$$p = \begin{cases} (h - r) \cdot k_n & \text{if } h - r > 0 \\ 0 & \text{if } h - r \leq 0, \end{cases} \tag{1}$$

The friction formulation is obtained from Abaqus Theory Guide [48], where it is referred to as 'elastic stick formulation'. Elastic (reversible) slip components γ_i^{el} are permitted so that the equivalent elastic slip does not exceed a critical value γ_{crit} that is defined by the user. This formulation has finite tangential stiffness k_t in stick condition dependent on critical elastic slip and critical shear traction, as shown in Eq. (2). The critical shear traction for slip limit τ_{crit} depends on the contact pressure p and COF μ according to Eq. (3). In stick condition, components of the 'current' shear traction are defined as the product of tangential stiffness and elastic slip components according to Eq. (4).

$$k_t = \frac{\tau_{crit}}{\gamma_{crit}}, \tag{2}$$

$$\tau_{crit} = \mu p. \tag{3}$$

$$\tau_i = k_t \gamma_i^{el}. \tag{4}$$

$$\tau_{eq} = \sqrt{\tau_1^2 + \tau_2^2}. \tag{5}$$

Equivalent shear traction can be calculated from shear traction components τ_1 and τ_2. Slip occurs if the equivalent shear traction defined in Eq. (5) exceeds τ_{crit}. In that case an 'irreversible' slip $\Delta\gamma_{eq}^{sl}$ has to be considered so that $\tau_{eq} = \tau_{crit}$. The direction of the shear traction is considered to be parallel to the slip increment direction meaning isotropic COF. The relation of shear traction, elastic slip, and irreversible slip is illustrated in Figure 2. $\Delta\gamma_{eq}^{pr}$ is an 'elastic predictor' that is used in the iteration scheme of Abaqus. Finally, the 'irreversible' slip increment can be solved according to Eq. (6). Described equations and linearization of the problem for iterative solution scheme can be found from Abaqus Theory Guide [48].

$$\Delta\gamma_{eq}^{sl} = \gamma_{eq}^{pr} - \gamma_{crit}. \tag{6}$$

There is no general theory to describe the COF evolution under fretting conditions but results from constant pressure fretting tests performed by Hintikka et al. [25] show that either accumulated sliding distance or frictional energy dissipation can be used as the driver for evolution. The latter one was selected to define the COF evolution because it conveniently includes the effect of contact pressure and slip. Energy-based criteria and thresholds are commonly used in fretting models [13, 14, 17]. For example, the well-known Ruiz criterion [13] and its modifications use the frictional energy variable to describe surface damage. Vidner and Leidich [14] have presented that part of the frictional energy is consumed to adhesion, micro-welding, and small surface crack formation. Based on these findings the COF for analysis increment n is defined as

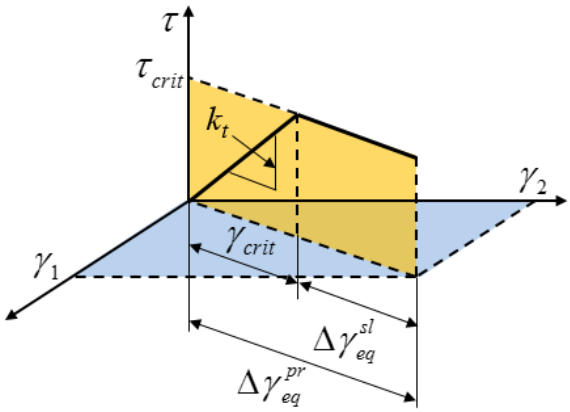

Figure 2: Computation of incremental slip.

$$\mu_{n+1} = \begin{cases} \mu_n + k \cdot \Delta\gamma_{eq}^{sl} \cdot \tau_{eq} & \text{if} \quad \mu_{n+1} < \mu_{max} \\ \mu_{max} & \text{if} \quad \mu_{n+1} \geq \mu_{max}, \end{cases} \tag{7}$$

where k is a constant defining the rate of friction coefficient increase and μ_{max} is the maximum allowed value of the COF. Wear depth r is defined according to Archard's law [35] as

$$r_{n+1} = \begin{cases} r_n + w \cdot \Delta\gamma_{eq}^{sl} \cdot p & \text{if } p \geq p_{lim} \\ r_n & \text{if } p < p_{lim}, \end{cases} \tag{8}$$

where w is a constant controlling the rate of wear, p is contact pressure, and p_{lim} is an optional limit value below which the wear does not occur.

As seen from Eq. (7), the COF can only increase during the analysis from the initial value up to a maximum corresponding to the measured stable friction limit [26]. The goal is to find out whether the contact stabilizes to a safe condition, meaning stick condition with maximum allowed COF. Considering only the evolution of COF (not wear), this means that contact condition evolves from gross or partial slip to stick but not vice versa. If the contact slides with maximum allowed COF, it can be predicted that COF would temporarily rise to higher unstable values and fretting scars or adhesion spots form in the sliding area [25, 26].

The effect of wear on the contact condition is different, and the main interest is the consequence of wear in partial slip condition. Depending on the wear volume and stiffness of the structure, contact can either evolve to gross slip and loosen or shakedown to full stick condition where part of the contact interface is damaged. Cases, where wear has led to full stick condition, are notch-like problems and can be furthermore analyzed by using fatigue criteria or fracture mechanics to evaluate the integrity of the joint. However, analyzing this further is not in the scope of this paper. The combined effect of both COF development and wear on contact condition, and surface damage is illustrated in Figure 3. As the purpose of this approach is to find stabilized conditions, realistic rates of evolution are not considered, but history dependency of the μ and r needs to be captured. The ratio between k and w defines the competition between COF evolution and wear and has a strong influence on the results. To simplify this problem, an assumption, that the evolution of COF is much faster compared to wear (i.e. $k \gg w$), is made based on the experimental evidence [24, 25].

2.2. Finite element models

Basic principles of the FE-models for all three cases, cylinder-on-plane (Fig.4a), bolted double beam (Fig.4b) and crankshaft-counterweight (CW) are the same. In all models, the surface-to-surface discretization and finite sliding contact tracking were used. Loading of the cylinder-on-plane and bolted double beam are described by using normal force or bolt tightening to generate the contact pressure and sinusoidal cyclic displacement to generate shear traction and slip. The cylinder-on-plane model is made to match with the model in [50], where Arnaud et al. have simulated

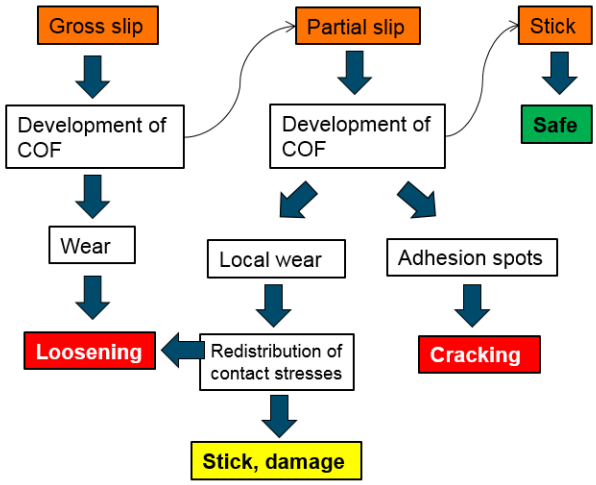

Figure 3: Effect of COF development and wear on contact condition and surface damage.

wear. In the bolted double beam, linear hexahedral elements with incompatible modes C3D8I were used. The mesh sizes in the contact zone were 0.04 mm for the cylinder-on-plane and 1 mm for the double beam. Linear C3D8I element type was chosen as it provides smooth contact results and rapid contact convergence and is also a good compromise between solution speed and accuracy. In the double beam, a finer mesh would be needed to capture the stress field in the material accurately, but it is not seen necessary in the context of macroscopic contact mechanics. In the case of further fatigue or crack propagation analysis, sub-modelling or refined models should be used after the contact simulation. The crankshaft-counterweight model was meshed by using 2nd order tetrahedrons C3D10. The loading of the counterweight model is more complicated as it comes from the flexible multibody simulation described in section 2.3. Loading of the CW model consists of displacements and acceleration fields in the time domain, which describe the full dynamics of the crankshaft. A similar process of connecting rod stress analysis is described in more detail in [45]. Details of the loading and FE-model of the CW contact are confidential.

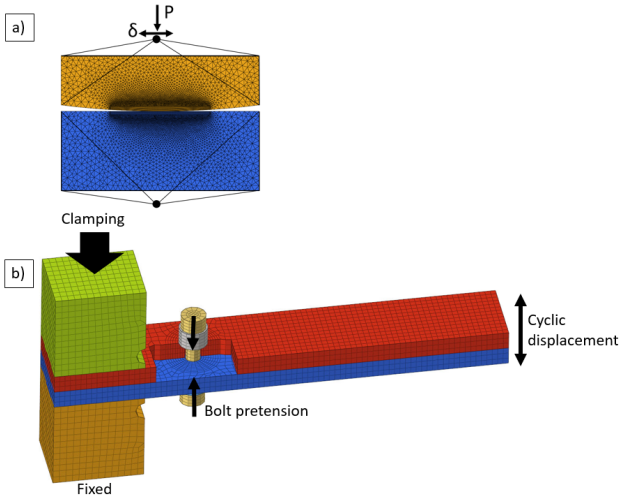

Figure 4: FEM models of cylinder-on-plane (a) and bolted double beam test (b).

2.3. Multibody simulation

Large medium-speed combustion engines have counterweights (CWs) bolted to the crankshaft due to the large size of the components. The bolted contacts of the CWs are loaded by the torsional and longitudinal vibrations of the crankshaft and centrifugal force. High frequency (>100 Hz) excitation is mainly caused by gear trains in the engine's power system. The dynamics of the CW is very complicated but can be simulated by using a modern flexible MBS model shown in Fig.5a. Similar MBS models are described in more detail in [44, 51]. The MBS model was validated by acceleration measurements in a running engine by using the measurement device described in [52]. The main cyclic shear loading of the CW contact is caused by the natural vibration mode where CW wings are vibrating in the longitudinal direction of the engine in the opposite phase with each other. This so-called "torsion" mode and its simulated and measured vibration spectrum are shown in Fig.5c. Furthermore, non-linear FEM analysis of the CW contact was accomplished by applying loadings from the MBS simulation (Fig.5b).

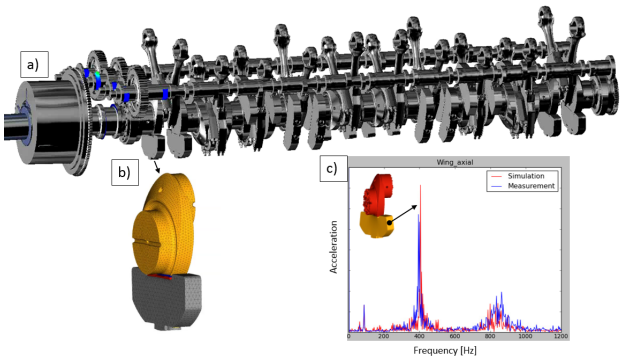

Figure 5: MBS model of engine powertrain (a), counterweight FEM model (b) and simulated and measured counterweight vibration spectrum (c).

3. Results and Discussion

3.1. Contact model validation

The contact and wear model were tested by simulating the cylinder-on-plane wear test described in detail in [50] by using constant COF. Material pair was Ti-6Al-4V with the elastic modulus of 120 GPa, Poisson's ratio of 0.3, and yield strength of 880 MPa. Cylinder radius was 80 mm, and normal force 1066 N/mm. Due to compliance of the model, 87 micron tangential displacement at reference point connected to cylinder (Fig. 4a) was needed with COF 0.56 to obtain a slip amplitude of 75 micron. The wear model defined in Eq. (8) was modified so that the contact pressure was replaced by frictional shear traction to match with the model in [50]. The pressure limit for wear was set to zero. In the contact model, normal stiffness was 4 x 10^6 N/mm^3 and elastic slip 1 micron. Presented contact model does not consider different wear coefficients for each contacting bodies so wear coefficients 0.47 x 10^{-5} mm^3/J and 1.5 x 10^{-5} mm^3/J were summed to 1.97 x 10^{-5}mm^3/J. The results shown in Fig. 6 correspond well with the simulation results without the effect of the third body layer in [50]. Based on experimental findings in [50], the third body layer should be considered in the wear model, which means that the presented wear model is very limited. However, this study shows that the presented approach provides reasonable results without modifying the geometry (finite element mesh) because of wear. Of course, for much larger wear depths, geometry should be updated.

3.2. Double beam results

First, the described methodology is applied to the double beam fretting test described in [53]. In the double beam test, two beams are clamped together with a bolt, and the cyclic shear force and slip near the bolt hole are introduced by enforced cyclic displacement at the end of the beams. In this case, the material of the beams was quenched and tempered steel. The double beam setup and contact pressure distribution, with a 30 kN bolt tightening force, are shown in Fig. 7.

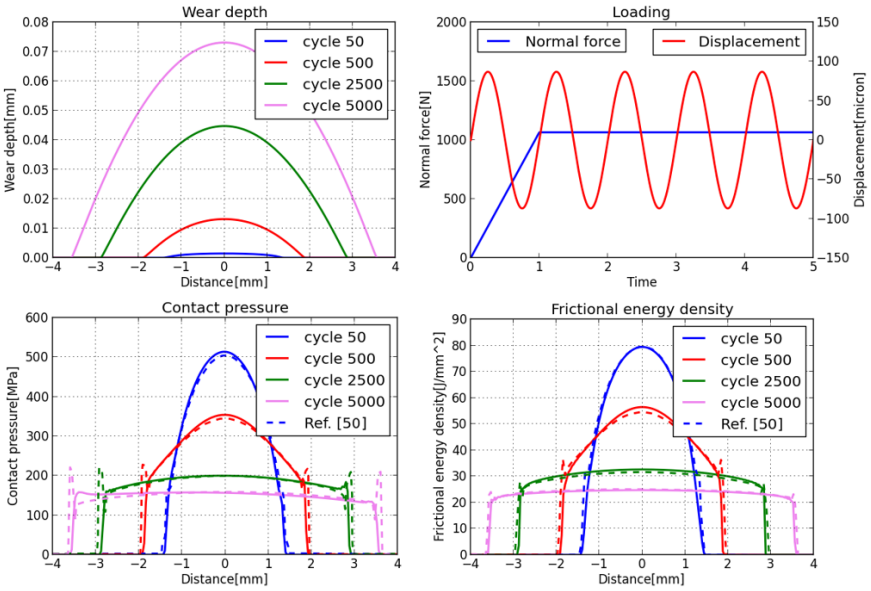

Figure 6: Wear simulation results and load definition of cylinder-on-plane model. Dashed line corresponds to digitized data from [50], the model without consideration of third body layer.

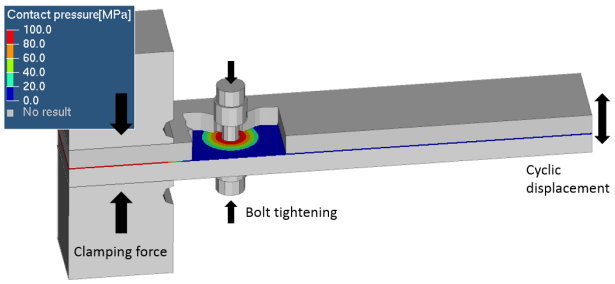

Figure 7: The double beam fretting apparatus with contact pressure distribution. Color image is available in the online version.

Two different load cases were selected from the measurement matrix described in Juoksukangas et al. [53], which are here referred to as ”low slip” and ”high slip” cases. The low slip case has bolt force 30 kN and displacement amplitude of the free end of the cantilever beam 1.4 mm corresponding to nominal bending stress of 130 MPa at the hole location. The high slip case has the corresponding parameters 20 kN, 2.3 mm, and 205 MPa. The maximum value allowed for COF is the most critical parameter affecting the stabilized contact condition. Hintikka et al. [26] have measured that the stable friction threshold is 0.7 at the outer edge of the annular flat-on-flat contact for the same material pair. The same value is used here as the maximum value COF can achieve (μ_{max}). The first 100 simulation cycles were used to find stabilized COF distribution, followed by the wear simulation. The stabilized COF distribution and rate of frictional energy dissipation after 100 cycles are plotted in Fig.8.

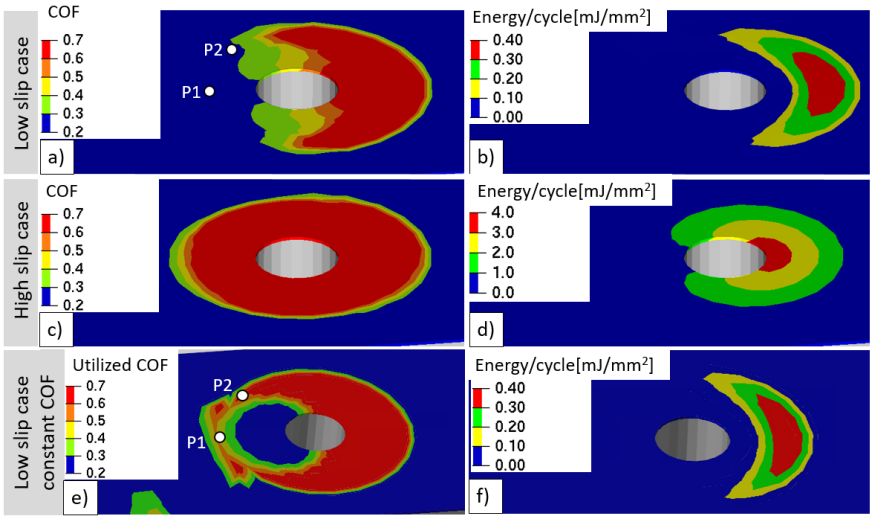

Figure 8: Stabilized COF distribution and rate of frictional energy dissipation after 100 cycles in low slip case (a,b) and high slip case (c,d). Corresponding results with constant COF in low slip case (e,f). Color image is available in the online version.

In the low slip case, the COF reaches its maximum value in front of the bolt hole (Fig.8a) and remains sliding in the area where frictional energy dissipation is greater than zero (Fig.8b). The COF has not increased behind the hole from the initial value of 0.2, which indicates that the contact has been in partial slip condition from the beginning of the simulation. Slip range distributions can be seen in more detail in Fig.9a. The stabilized slip area corresponds well to the experimental fretting scars shown in Fig.10a.

In the high slip, case the COF evolves in the whole area of contact, which reveals that the contact was initially in gross slip condition. The stabilized COF distribution after 100 simulation cycles shown in Fig.8c and the rate of frictional energy dissipation after 100 cycles in Fig.8d show that the contact has evolved to partial slip condition. The contact is very close to the gross slip condition, which can be seen from the slip range distribution in Fig.9b. The contact is in stick only at the edge of the bolt hole. Again, the remaining slip area corresponds well with the experimental fretting scars shown in Fig.10b. These results support the hypothesis that the area, where the contact remains sliding after the local COF has developed to its stable limit value, is expected to show surface damage, clear and substantial fretting scars, and adhesion spots. In practice, the majority of the designs can be validated by analyzing the COF evolution, possible wear area, and the effects on the clamping force. Stabilized COF distribution in stick condition reveals the safety margin; how much the shear/pressure relationship can increase before fretting damage starts to occur and is therefore valuable for the assessment of design robustness.

The low slip case was also simulated using constant COF of 0.7, for comparison. The rate of frictional energy dissipation field is very similar compared to the field obtained using spatially evolving COF (Fig.8f). This means that the slip in the double beam experiment is not sensitive to non-uniform COF, which is usually the case in displacement controlled stiff structures. Utilized COF (Fig.8e), defined as the frictional shear traction divided by the contact pressure, is different from fully evolved COF (Fig.8a). With constant COF, the utilization of COF is significantly higher behind the bolt hole. The difference stems from the lack of history dependency of frictional shear traction. When the

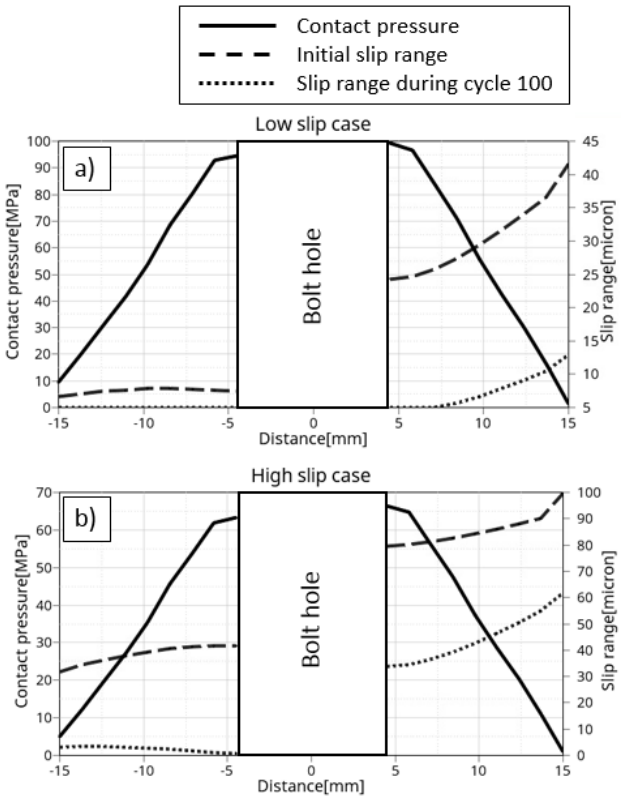

Figure 9: Contact pressure and slip ranges along path in the direction of the beams in the low slip case (a) and high slip case (b).

COF rises faster in front of the bolt hole, this area carries a bigger portion of the shear load, simultaneously reducing it from the other side of the hole. Maximum shear traction during the 100th cycle was measured from the same locations in both models, marked as P1 and P2 in Fig. 8a and Fig.8e. The maximum shear tractions in the variable COF model were 3.3 MPa (P1) and 3.7 MPa (P2). Corresponding values in the constant COF model were 5.5 MPa (P1) and 6.0 MPa (P2).

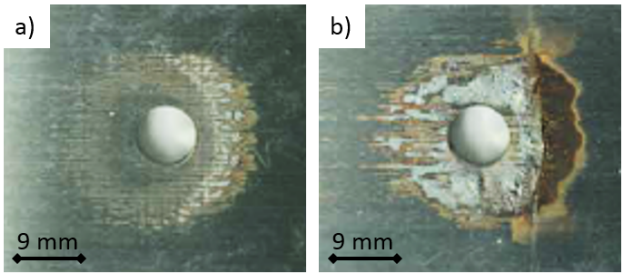

Figure 10: Experimental fretting damage in the low slip case (a) and the high slip case (b). Color image is available in the online version.

The wear simulation was activated after 100 simulation cycles, and results are shown in Fig.11. In the low slip case, the contact shakes down to a fully stuck state, and the contact pressure concentrates near the bolt hole. The wear area is larger than the slip area before wear as the wear reduces the clamping force of the joint, which consequently increases the slip and wear area. Wear depth and contact pressures are plotted along a path in the axial direction over the bolt hole in Fig.12a. There is approximately 1 kN reduction in the bolt force (Fig.13a) in the low slip case, and the joint remains functional. Of course, fatigue analysis should be performed to ensure that cracks do not initiate at the border of the worn contact. According to the experimental findings, the wear does not seem to play a significant role in this case, and that also reveals the limitations of the current wear model. In reality, the material does not disappear from the contact but is entrapped or ejected from the contact borders. Future investigation is needed to develop a more realistic wear model, but the presented approach still provides a conservative approach for engineering purposes.

In the high slip case, the contact evolved from gross slip to partial slip during the first 100 cycles. During the wear simulation, only a small area behind the bolt hole is sticking. In this case, the clamping force starts to reduce, as shown in Fig.13b. As wear progresses, the small area in stick cannot anymore carry the shear load without sliding. The contact condition changes back to gross slip as the wear continues, and the clamping force reduces meaning that the contact loosens eventually. At this point, it is clear that the contact conditions are not improving, and the analysis can be stopped. Comparison to the experimental findings in Fig.10b reveals that there has been severe material transfer between the bodies, but the contact has not worn as the simulation predicted. This again shows the limitations of the presented wear model. This experiment was stopped after the major crack had propagated, which has affected the visuals of the surface damage of the joint captured at the end of the test.

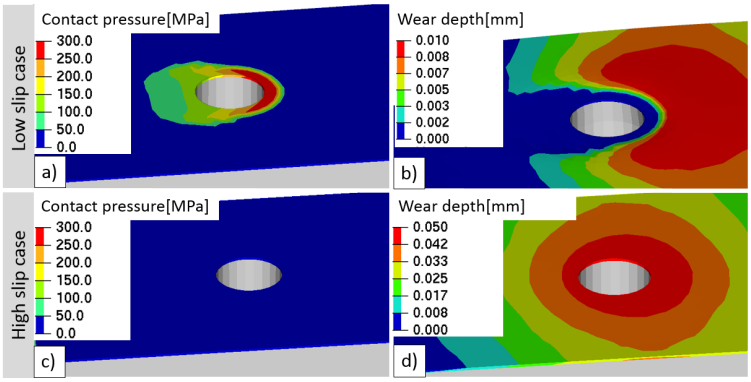

Figure 11: Contact pressure and wear depth of the low slip case (a,b) and the high slip case (c,d). Color image is available in the online version.

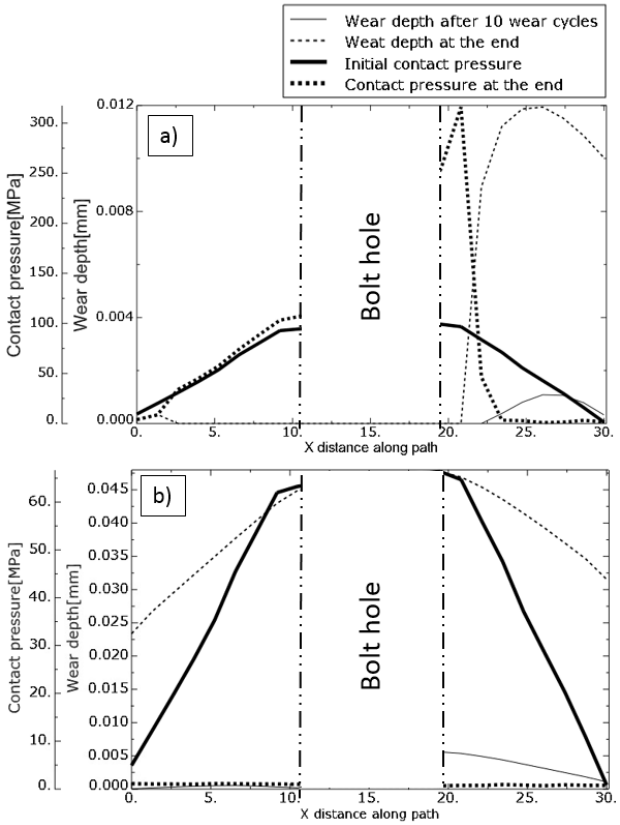

Figure 12: Wear depth and contact pressure along path in the low slip case (a) and high slip case (b).

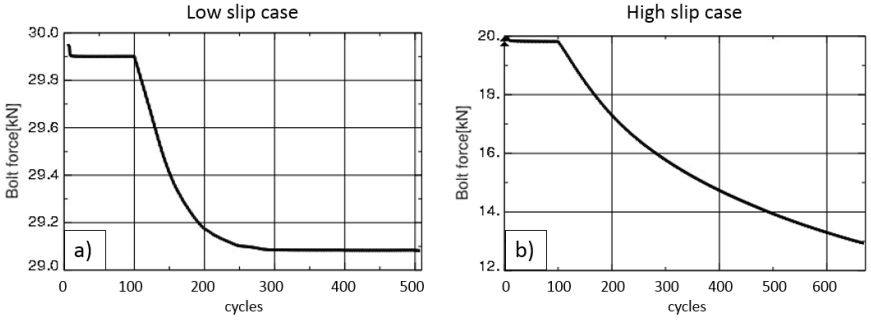

Figure 13: Bolt force development of the low slip case (a) and the high slip case (b).

3.3. Counterweight case study

Detailed geometry of the contact between the crankshaft and CW cannot be revealed in this paper, but the contact consists of two similar flat surfaces loaded by the bolt tightening, centrifugal force, and ”torsion” mode vibration causing the cyclic shear force in the contact. Loading of the CW, its contact area and contact pressure distribution are shown in Fig.14. Bolt forces and centrifugal force is constant and the wing vibration sinusoidal. Contact pressure is in the yield limit at the contact edges. When the CW wing vibrates back and forth, the movement causes a cyclic shear force to the contact, which can lead to slip first at the edge near the wing (Fig14). In normal engine operating conditions, the contact is very safe, meaning full stick with the wing vibration of 100 microns. Therefore the simulation was run at severe overload of the engine, that is not practically possible in reality. This means overestimation of wing movement amplitude up to 230 microns in ‘severe overload’ case and 300 microns in the ‘extreme overload’ case. This was done to find the safety limit of the design in terms of CW wing vibration. In practice, this is possible only by using simulation as failing contact of this type would lead to catastrophic failure of the engine and possibly its surroundings. The simulation principle is the same as in double beam fretting test case but more conservative value of maximum allowed COF is used. The maximum COF was limited to 0.5 that has been measured to be the average maximum value of the contact area in the experimental results in [26]. 250 load cycles were simulated to find the stabilized COF distribution before the activation of wear.

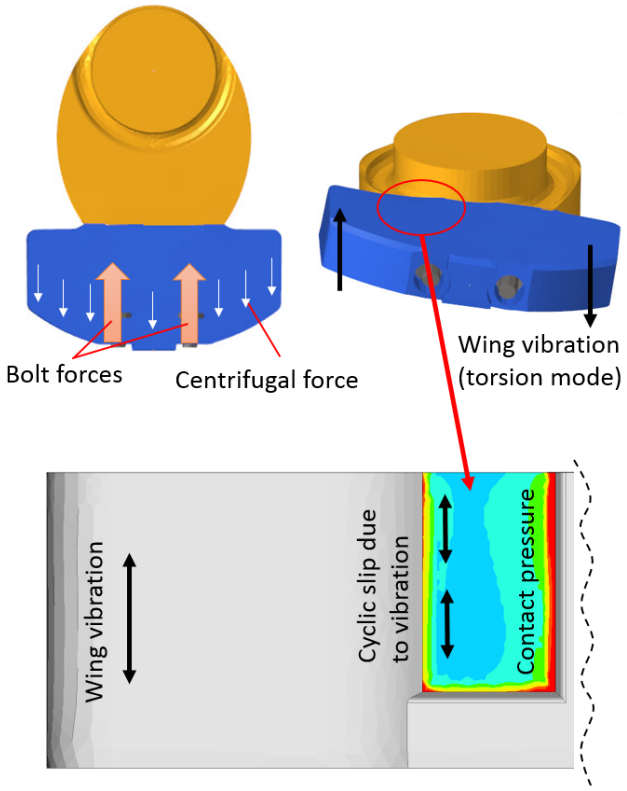

Figure 14: One of the CW contact area and its contact pressure distribution.

Fig.15a shows the stabilized COF distribution before wear, and it can be seen that COF has increased in large areas of the contact, which also reveals the slip area in the beginning. Slip amplitude before the evolution of COF was about 5 micron at the contact edge. The contact is initially in partial slip and practically shakes down to full stick condition. There is one node at the corner where a small amount of slip occurs, but in practice, it is insignificant, and further wear simulation is not required. The contact, in this case, can be deemed safe against fretting damage.

In the extreme loading case, the contact is also initially in partial slip. Slip amplitude at the contact edge near the wing is about 30 micron. After 250 cycles the COF has increased in about 70% area of the contact (Fig.16a).

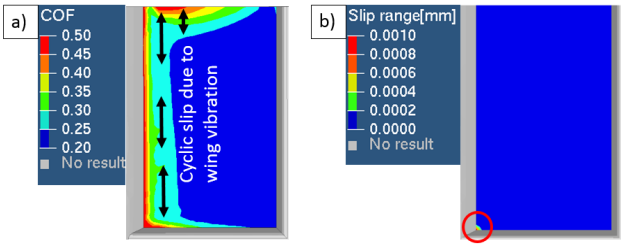

Figure 15: Stabilized COF distribution (a) and slip range (b) of the severe overload case. Color image is available in the online version.

After stabilized COF, the contact remains in partial slip condition (Fig.16b). In this case, it is useful to simulate the effect of wear. The slip area after COF evolution is large enough to reduce the clamping force of the contact by wear to such degree that the slip area starts to grow. This consequently leads to the growth of the worn area, and the contact shows signs of loosening. After 1300 simulation cycles, approximately 75% of the contact area has worn (16d) and completely lost contact pressure (16c). The clamping force has dropped by approximately 30%, and the wear simulation could be continued, but it is already clear that this situation is not acceptable anymore. Furthermore, the bolt force evolution during the wear simulation in Fig.17 shows no signs of stabilization, which is another indicator of eventual catastrophic failure. From engineering point of view, it is safe to have 230 micron vibration amplitude at the CW wing as the contact evolves to stuck condition. 300 micron vibration amplitude at the CW wings would lead to contact loosening and eventually failure of the bolts. Practically this means that the CW would fly out from the engine.

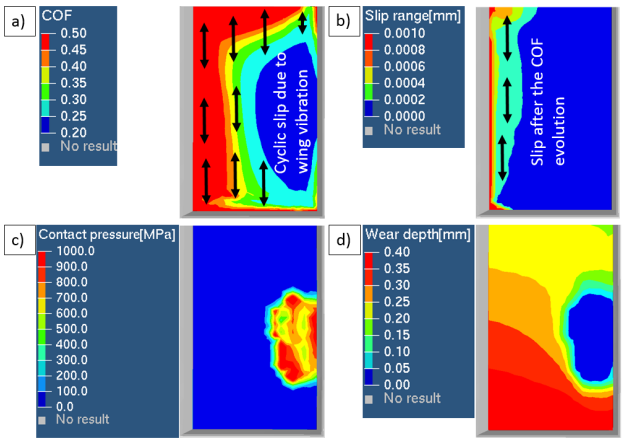

Figure 16: Stabilized COF distribution (a) and slip distribution (b) after 250 simulation cycles. The contact pressure (c) and wear depth (d) after 1300 simulation cycles. Color image is available in the online version.

4. Conclusion

A contact model to consider local COF evolution and wear under fretting conditions is implemented for Abaqus FEM solver. The presented method enables the simulation of changes in the contact condition between gross slip, partial slip, and stick condition due to increasing COF and material removal due to wear. The stable maximum COF concept was used to predict the contact condition before wear and also to determine if surface damage occurs. Classic Archard's wear model was employed to describe material removal. The method was applied to the cylinder-on-plane wear experiment, bolted joint fretting test case and contact between large crankshaft and counterweight. Following conclusions were made:

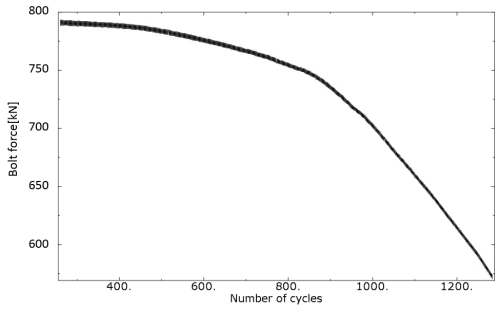

Figure 17: Bolt force of the extreme overload case as a function of cycles during wear simulation.

- The numerical contact model was validated against a cylinder-on-plane wear experiment. The presented method provides similar results obtained with a simulation where geometry is updated due to wear. This validates the contact subroutine and the approach where the wear profile is considered in the contact pressure calculation without updating the geometry, at least for relatively small wear depths.
- Stabilized COF distribution, together with the remaining slip area, seems to work as a surface damage criterion under fretting conditions. Areas where sliding occurs, where the local COF has evolved to its maximum limit value, are expected to show fretting scars or adhesion spots. Simulation results of the bolted joint fretting test case compared to the experimental inspection of the contact qualitatively support this hypothesis.
- Archard's wear model is too simple, as it does not consider the wear particle entrapment inside the contact. Instead, it assumes that the wear debris vanishes from the contact, which does not seem to be the case. Nevertheless, the presented wear model can give a conservative estimate of the contact loosening and eventual failure or shakedown to stick condition.
- The presented method is applicable to industrial-scale simulation to support the design of large machine components. More fretting testing is required to validate the limit values for safe, stable COF, especially at different contact pressures. More physical wear model, other COF evolution models, and surface damage criteria also require further investigation.

5. Acknowledgements

This work is a part of the MaNuMiES (Dnro 3361/31/2015) and WIMMA (Dnro 1566/31/2015) research projects. The authors are grateful for the financial support provided by Business Finland Oy, Wärtsilä Finland Oy, Agco Power Oy and Global Boiler Works Oy. The authors also want to thank peer reviewers who did great work helping to improve the quality of the paper.

References

[1] R. Waterhouse, Fretting corrosion, Pergamon press, Oxford, ISBN 0 08 16902 3, 1972.
[2] K. Johnson, Contact Mechanics, Cambridge University Press, Cambridge, 1985.
[3] D. Hills, D. Nowell, Mechanics of fretting fatigue, 1994.
[4] R. Rabb, Todennäköisyysteoriaan pohjautuva väsymisanalyysi, BoD-Books on Demand, Helsinki, Finland (2013).
[5] J. Vaara, A. Mäntylä, T. Frondelius, Brief review on high-cycle fatigue with focus on non-metallic inclusions and forming, Rakenteiden Mekaniikka 50 (2017) 146–152.
[6] M. Väntänen, J. Vaara, J. Aho, J. Kemppainen, T. Frondelius, Bayesian sequential experimental design for fatigue tests, Rakenteiden Mekaniikka 50 (2017) 201–205.
[7] R. Rabb, Fatigue failure of a connecting rod, Engineering Failure Analysis 3 (1996) 13 – 28.
[8] M. Baietto, E. Pierres, A. Gravouil, B. Berthel, S. Fouvry, B. Trolle, Fretting fatigue crack growth simulation based on a combined experimental and {XFEM} strategy, International Journal of Fatigue 47 (2013) 31 – 43.
[9] A. de Pannemaecker, S. Fouvry, B. Berthel, J.-Y. Buffiere, Numerical methods for stress intensity factor ΔK calculations of fretting cracked interface, Tribology International 119 (2018) 389 – 403.

[10] M. Kubota, S. Kataoka, D. Takazaki, Y. Kondo, A quantitative approach to evaluate fretting fatigue limit using a pre-cracked specimen, Tribology International 108 (2017) 48 – 56.
[11] K. Pereira, M. A. Wahab, Fretting fatigue crack propagation lifetime prediction in cylindrical contact using an extended MTS criterion for non-proportional loading, Tribology International 115 (2017) 525 – 534.
[12] S. Fouvry, D. Nowell, K. Kubiak, D. Hills, Prediction of fretting crack propagation based on a short crack methodology, Engineering Fracture Mechanics 75 (2008) 1605 – 1622.
[13] C. Ruiz, P. Boddington, K. Chen, An investigation of fatigue and fretting in a dovetail joint, Experimental Mechanics (1984).
[14] J. Vidner, E. Leidich, Enhanced ruiz criterion for the evaluation of crack initiation in contact subjected to fretting fatigue, International Journal of Fatigue (2007).
[15] M. Zehsaz, P. Shahriary, The effects of friction coefficient and interference on the fretting fatigue strength of railway axle assembly, UPB Scientific Bulletin, Series D: Mechanical Engineering 75 (2013).
[16] V. Nurmi, J. Hintikka, J. Juoksukangas, M. Honkanen, M. Vippola, A. Lehtovaara, A. Mäntylä, J. Vaara, T. Frondelius, The formation and characterization of fretting-induced degradation layers using quenched and tempered steel, Tribology International 131 (2019) 258 – 267.
[17] C. Jiménez-Peña, R. H. Talemi, B. Rossi, D. Debruyne, Investigations on the fretting fatigue failure mechanism of bolted joints in high strength steel subjected to different levels of pre-tension, Tribology International 108 (2017) 128 – 140.
[18] N. A. Bhatti, K. Pereira, M. A. Wahab, A continuum damage mechanics approach for fretting fatigue under out of phase loading, Tribology International 117 (2018) 39 – 51.
[19] J. Araujo, L. Susmel, M. Pires, F. Castro, A multiaxial stress-based critical distance methodology to estimate fretting fatigue life, Tribology International 108 (2017) 2 – 6.
[20] B. Zhao, F. Shen, Y. Cui, Y. Xie, K. Zhou, Damage analysis for an elastic-plastic body in cylindrical contact with a rigid plane, Tribology International 115 (2017) 18 – 27.
[21] C. Gandiolle, S. Garcin, S. Fouvry, A non-collinear fretting-fatigue experiment to compare multiaxial fatigue criteria: critical shear plane strategy is better than invariant formulations, Tribology International 108 (2017) 57 – 68.
[22] L. Vincent, Y. Berthier, M. Dubourg, M. Godet, Mechanics and materials in fretting, Wear 153 (1992) 135 – 148.
[23] A. Pasanen, S. Järvisalo, A. Lehtovaara, R. Rabb, Development of a test device for the evaluation of fretting in point contact, Lubrication Science 21 (2009) 41–52.
[24] J. Hintikka, A. Lehtovaara, C. Lönnqvist, Effect of start-up schemes and amplitude of tangential motion on friction behavior in fretting point contact, Tribology International 44 (2011) 1535–1543.
[25] J. Hintikka, A. Lehtovaara, A. Mäntylä, Fretting-induced friction and wear in large flat-on-flat contact with quenched and tempered steel, Tribology International 92 (2015) 191–202.
[26] J. Hintikka, A. Mäntylä, J. Vaara, T. Frondelius, A. Lehtovaara, Stable and unstable friction in fretting contacts, Tribology International 131 (2019) 73 – 82.
[27] J. Hintikka, A. Lehtovaara, T. Frondelius, A. Mäntylä, Tangential traction instability in fretting contact below fully developed friction load, Rakenteiden mekaniikka 50 (2017) 175–178.
[28] T. Yue, M. A. Wahab, Finite element analysis of fretting wear under variable coefficient of friction and different contact regimes, Tribology International 107 (2017) 274 – 282.
[29] S. Naboulsi, T. Nicholas, Limitations of the coulomb friction assumption in fretting fatigue analysis, International Journal of Solids and Structures 40 (2003) 6497 – 6512.
[30] M. Cheikh, S. Quilici, G. Cailletaud, Presentation of KI-COF, a phenomenological model of variable friction in fretting contact, Wear (2007).
[31] M. Godet, The third-body approach: a mechanical view of wear, Wear 100 (1984) 437–452.
[32] Y. Berthier, L. Vincent, M. Godet, Velocity accommodation in fretting, Wear 125 (1988) 25–38.
[33] R. Merhej, S. Fouvry, Contact size effect on fretting wear behaviour: application to an AISI 52100/AISI 52100 interface, Lubrication Science 21 (2009) 83–102.
[34] A. Warmuth, S. Pearson, P. Shipway, W. Sun, The effect of contact geometry on fretting wear rates and mechanisms for a high strength steel, Wear 301 (2013) 491 – 500. Wear of Materials 2013.
[35] J. F. Archard, Contact and rubbing of flat surfaces, Journal of Applied Physics 24 (1953) 981–988.
[36] T. Hattori, K. Yamashita, Y. Yamashita, Simple estimation method of fretting fatigue limit considering wear process, Tribology International 108 (2017) 69 – 74.
[37] J. Madge, S. Leen, I. McColl, P. Shipway, Contact-evolution based prediction of fretting fatigue life: effect of slip amplitude, Wear 262 (2007) 1159–1170.
[38] O. Vingsbo, S. Söderberg, On fretting maps, Wear 126 (1988) 131–147.
[39] D. Hills, A. Sackfield, R. Paynter, Simulation of fretting wear in halfplane geometries: Part 1—the solution for long term wear, Journal of Tribology 131 (2009) 031401–031401–4.
[40] I. Argatov, Y. Chai, Limiting shape of profiles in fretting wear, Tribology International 125 (2018) 95–99.
[41] A. Lehtovaara, C. Lönnqvist, Modelling and analysis of fretting wear in rough point contacts in partial slip conditions, Proceedings of the Institution of Mechanical Engineers, Part J: Journal of Engineering Tribology 225 (2011) 986–998.
[42] T. Frondelius, H. Tienhaara, M. Haataja, History of structural analysis & dynamics of wärtsilä medium speed engines, Rakenteiden Mekaniikka 51 (2018) 1–31.
[43] J. Könnö, H. Tienhaara, T. Frondelius, Wärtsilä digital design platform, Rakenteiden Mekaniikka 50 (2017) 234–238.
[44] T. Frondelius, P. Halla-aho, A. Mäntylä, Crankshaft development with virtual engine modelling, in: CIMAC Congress Helsinki.
[45] J. Göös, A. Leppänen, A. Mäntylä, T. Frondelius, Large bore connecting rod simulations, Rakenteiden Mekaniikka 50 (2017) 275–278.
[46] A. Mäntylä, J. Göös, A. Leppänen, T. Frondelius, Large bore engine connecting rod fretting analysis, Rakenteiden Mekaniikka 50 (2017) 239–243.
[47] J. Juoksukangas, V. Nurmi, J. Hintikka, M. Vippola, A. Lehtovaara, A. Mäntylä, J. Vaara, T. Frondelius, Characterization of cracks formed in large flat-on-flat fretting contact, International Journal of Fatigue 124 (2019) 361 – 370.

[48] D. Systèmes, Abaqus Theory Manual, 2012.
[49] M. E. Kartal, D. M. Mulvihill, D. Nowell, D. A. Hills, Measurements of pressure and area dependent tangential contact stiffness between rough surfaces using digital image correlation, tribology International 44 (2011) 1188–1198.
[50] P. Arnaud, S. Fouvry, S. Garcin, A numerical simulation of fretting wear profile taking account of the evolution of third body layer, Wear 376-377 (2017) 1475 – 1488. 21st International Conference on Wear of Materials.
[51] T. Kuivaniemi, A. Mäntylä, I. Väisänen, A. Korpela, T. Frondelius, Dynamic gear wheel simulations using multi body dynamics, Rakenteiden Mekaniikka 50 (2017) 287–291.
[52] P. Halla-aho, A. Mäntylä, T. Frondelius, T. Helander, J. Hautala, Counterweight measurements device development, Rakenteiden Mekaniikka 50 (2017) 318–322.
[53] J. Juoksukangas, A. Lehtovaara, A. Mäntylä, Experimental and numerical investigation of fretting fatigue behavior in bolted joints, Tribology International 103 (2016) 440–448.